

Design optimisation of Ironless Motors based on Magnet selection

M.C. Greaves*, G.R. Walker* & B.B. Walsh**

* School of Computer Science and Electrical Engineering
University of Queensland

** Tritium Pty. Ltd.

Abstract

This paper considers the design of a radial flux permanent magnet ironless core brushless DC motor for use in an electric wheel drive with an integrated epicyclic gear reduction. The motor has been designed for a continuous output torque of 30Nm and peak rating of 60Nm with a maximum operating speed of 7000 RPM.

In the design of brushless DC motors with a toothed iron stator the peak air-gap magnetic flux density is typically chosen to be close to that of the remanence value of the magnets used. This paper demonstrates that for an ironless motor the optimal peak air-gap flux density is closer to the maximum energy product of the magnets used. The use of a radial flux topology allows for high frequency operation and can be shown to give high specific power output while maintaining a relatively low magnet mass. Two-dimensional Finite Element Analysis is used to predict the air-gap flux density. The motor design is based around commonly available NdFeB bar magnet size.

List of Symbols

B_{peak}	= Magnetic Flux Density (T)
J_{rms}	= RMS Current Density (A/m ²)
J_{peak}	= Peak Current Density (A/m ²)
A_{active}	= Cross sectional area of winding (m ²)
L_{active}	= Active length of a pole (m)
D	= Diameter of the conductor (Litz wire)
N_{poles}	= Number of Magnet Poles
$N_{Conductors}$	= Total number of individual conductors
K_{ends}	= Increase in turn length due to end turns
ω	= Angular Velocity (rad/s)
V_{active}	= Active volume of copper in a pole (m ³)
ρ	= Resistivity of Copper (Ωm)

1. INTRODUCTION

The level of urban air pollution, global warming due to greenhouse gas production and the current rate of oil consumption are driving a revolution in automotive propulsion technologies. In recent years there has been the introduction of three hybrid electric vehicles by major automotive manufactures with a number of others to follow suit. These hybrid vehicles can provide a significant reduction in emission and fuel consumption, but they are really only an intermediate solution to truly sustainable transportation.

The technology that is predicted to be the future of vehicle propulsion is the fuel cell. A fuel cell is a device that converts a fuel directly to electricity that can then be used to power an electric drive system. Although there have been major break throughs in the construction of fuel cells in recent years the total cost of the entire drive train is still predicted to be significantly higher than that of the current internal combustion engine (ICE) and gearbox.

A Hypercar is a vehicle concept proposed by the Rocky Mountain Institute [1] to massively increase vehicle efficiency while not significantly increasing the vehicle's cost. The concept proposes a large reduction in both vehicle mass and aerodynamic drag. The resulting lower power required to drive the vehicle will result in a smaller, lighter drive train, which then further reduces the mass of the vehicle. This concept of mass decompounding and ultra low drag combined with low power accessories and highly efficient hybrid electric drive train is shown to result in a family vehicle with a fuel consumption of between 1-2 L/100km.

The University of Queensland has recently undertaken the design and development of a two-seater commuter vehicle that utilises the concept behind the Hypercar [2]. It has been proposed that the drive for this vehicle consist of two rear mounted

indirect drive wheel motors each capable of producing 22.5kW at 60km/hr, with a top speed of 120km/hr.

2. MOTOR REQUIREMENTS

Continuous Torque	30 Nm
Peak Toque	60 Nm
Maximum Speed	7000 RPM
Outer Diameter	Less than 300mm
Length	Less than 150mm
Weight	10 kg to 15 kg

Table 1. Basic machine requirements.

In the design of an efficient vehicle drive train the vehicle's driving cycle needs to be considered. In anything other than inner city driving a vehicle has low average power consumption compared to peak power requirements and hence a motor with high efficiency at high speed and low power levels is required. Due to the fact that this motor is to be used as a wheel mounted machine in a light-weight vehicle it is essential to keep the mass low to maintain a suitable ratio between the unsprung and the sprung mass of the vehicle. One motor that could possibly fit these requirements is a permanent magnet ironless core motor.

3. PM IRONLESS MACHINES

Since the introduction of high-energy magnets a number of papers have been present on the design and construction of permanent magnet (PM) brushless motors. Typically these designs demonstrate axial flux machines with a single central stator with magnets mounted on rotors on either side [3,4,5,6,7]. The absence of a steel core results in no iron core hysteresis losses and with the use of fine stranded Litz wire [4] the copper eddy current losses can also be minimised. These factors suggest that PM ironless machines can be designed for high frequency operation.

The electrical operating frequency of a motor is the product of the angular velocity of the machine and the number of magnetic pole pairs. It can be shown that when the number of poles of a machine is doubled the backing iron requiring is halved and the end turn length will also be reduced which combined will significantly lower the weight of an ironless machine. However there is a limit due to the fact that when the number of poles is increased for a given air-gap length the magnet Pole-Pole leakage field increases which leads to a increase requirement of magnetic material. This results in an optimal

number of poles for a given air gap diameter, winding volume and magnet thickness.

The angular velocity of the machine has been limited to 7000 RPM in order to allow the gear reduction to be made in a single step with an epicyclic gearbox. In an axial flux design retention of the magnets becomes a problem at high speeds.

For this reason it was decided that a radial flux configuration should be used instead of the typical axial flux topology. Fig. 1 shows a cross-section of the topology used for this motor. Note that the magnets are only placed on the inner diameter of the outer backing iron such that they will be able to withstand high-speed operation.

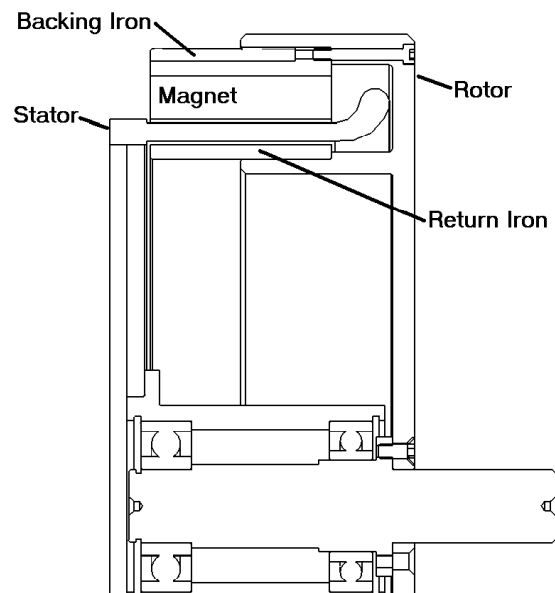


Fig. 1. Cross-Section of the PM Ironless machine.

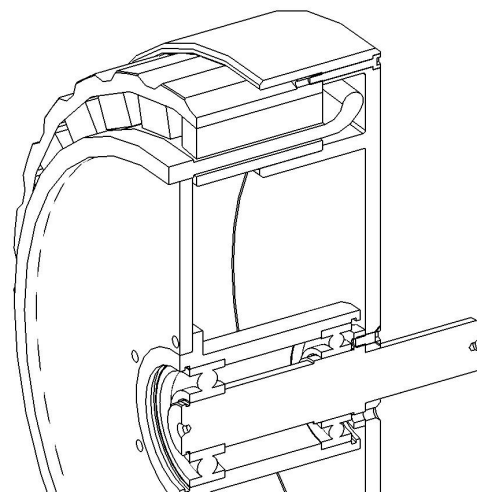


Fig. 2. 3-D Cross-Section of PM Ironless machine.

4. DESIGN OPTIONS

In the development of any motor there are a large number of variables to be consider to reach any level of optimisation. It was decided that this machine would employ 3 phases under 180-degree conduction with sinusoidal back-EMF. A spreadsheet was then developed which allowed the iterative process of motor design to be undertaken. The spreadsheet was combined with two-dimensional finite element analysis (Vector Fields OPERA-3d) to determine the magnetic field strength distribution at the centre of the air-gap and hence the back-EMF waveform. The major design variables that were considered were:

Major design variables

- Magnet dimensions
- The active axial length
- The peak magnetic flux density
- The back EMF wave form
- The number of poles
- The average radius of the air-gap
- The thickness of the stator
- The Mass of the machine
- Gauge of Litz wire

4.1 MAGNET DIMENSIONS

Typically the frame size of the motor will be one of the first variables that will be chosen. In this design the frame size of the machine was left relatively open and instead the variable that was fixed early in the motor design process was the magnet dimensions. The magnet was chosen from a list of commonly available NdFeB block sizes. The magnet size which was most suitable for the application measured 50mm x 20mm x 12 mm with the magnetisation direction passing through the 12mm thickness. This set the active axial length of the machine at 50mm.

4.2 THE PEAK MAGNETIC FLUX DENSITY AND THE BACK EMF WAVEFORM

Lumped circuit analysis was used to approximate the peak air-gap flux density during initial calculations. These calculations were then followed up by finite element analysis to evaluate if the flux distribution varies sinusoidally. Figure 3 shows a flux density plot for a single pole of the machine. The flux density alone a line through the centre of the air-gap was then plotted to form figure 4. This process was repeated for a number of air-gap lengths to accommodate various thickness stator, the peak flux density at each stator thickness was graphed (fig. 5)

to show the reduction in the field as the air-gap length is increased.

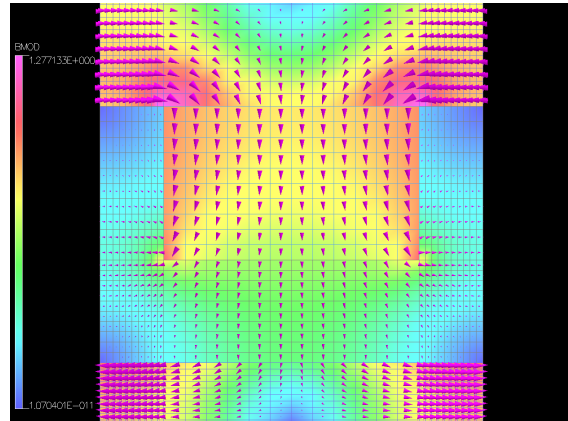


Fig. 3. Magnetic flux density (B) for a single pole.

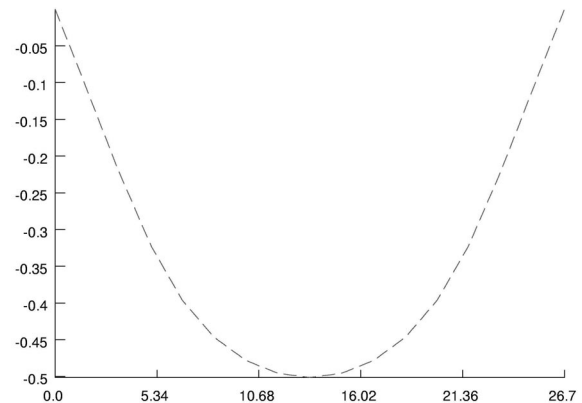


Fig. 4. Magnetic flux density (B) along the centre of the air-gap (mm).

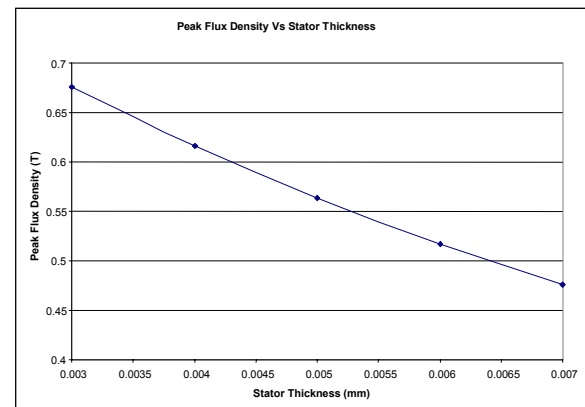


Fig. 5. The reduction of flux density (B) as the thickness of stator increases (mm).

4.3 NUMBER OF POLES, AVERAGE RADIUS AND THICKNESS OF THE STATOR

Analysis was carried out on an individual pole bases in order to determine an appropriate number of poles and optimal thickness. This could be done as the

magnet dimensions were kept constant and hence the pole dimensions and properties also remained constant.

For a pole of a radial flux ironless machine with sinusoidal back EMF and 180 degree conduction it can be shown that the force generated by a single pole F_{pole} is equal to:

$$F_{pole} = \frac{1}{2} B_{peak} J_{peak} V_{active} \quad (1)$$

Following on from this it can further be shown that the total torque that the machine will produce is equal to:

$$Torque = r F_{pole} N_{poles} \quad (2)$$

From equation (1) & (2) it can be seen that the active volume of copper and the radius at which it acts determines the torque output of an ironless machine.

In an ironless motor the larger the air gap the more space there is available for windings, however this is at the expense of the strength of the magnetic field density as seen in Figure 5. It can be shown (fig. 6) that although the magnetic field strength may reduce as the stator thickness is increased that the overall specific force (N/kg) per pole continues to increase for a given value of current density (A/m^2) in the windings. This is due to the increased current-carrying material in the air-gap.

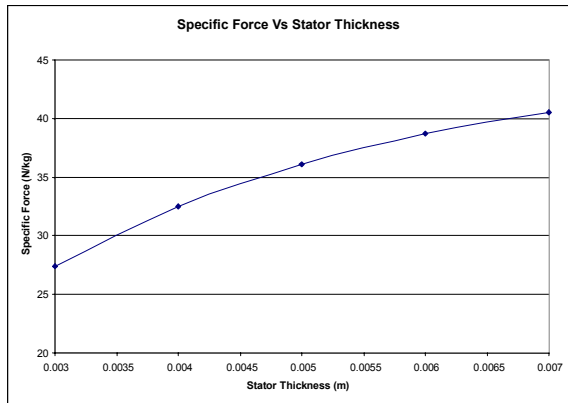


Fig. 6. Specific force per pole Vs stator thickness.

Figure 6 would suggest that a stator thickness of over 7mm should be employed, however this figure does not take into account the overall copper losses. Figure 7 shows an example of the total stator losses for the motor as the stator thickness is varied while maintaining the same active mass of the motor through increasing the number of poles.

The final design consists of 24 poles and a maximum operating frequency of 1400Hz. This

frequency is extremely high and requires a very high switching frequency controller to provide a smooth sinusoidal input current to the motor. A special controller is currently in being developed to control this machine and it is likely that it will employ either adaptive dead time switching or soft switching to reduce the switching losses of the controller mosfets. It is also worth noting that although the controller losses may increase it is much easier to remove heat from the controller than from an ironless machine mounted in a hub drive.

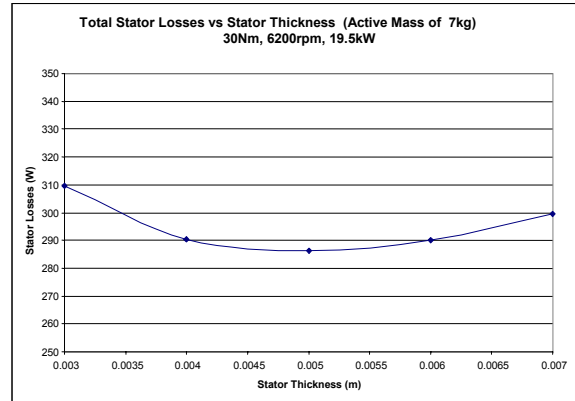


Fig. 7. Stator losses Vs stator thickness.

4.4 SELECTION OF LITZ WIRE GAUGE

Litz wire means woven wire in German and consists of a large number of individually insulated strands of wire woven together to form a larger effective wire gauge. Litz Wire was developed to help avoid skin effect in high frequency applications, but is also ideal for use in high frequency ironless motor applications as shown by Lovatt [4].

As each of the strands of wire are individually insulated the maximum achievable fill factor for Litz wire is low. This is offset, however, by the low resulting eddy current losses [8] at high operating frequencies. In order to select the most appropriate Litz wire gauge it is necessary to balance the increased resistive losses against the reduced eddy current losses as the wire gauge increases.

Resistive Losses in the stator

$$P_{Resistive} = I^2 R = \frac{(J_{rms} A_{active})^2 L_{active} K_{ends} \rho}{A_{active}} \quad (3)$$

Eddy Current Losses in the Stator

$$P_{Eddy} = \frac{\pi B_{peak}^2 \omega^2 D^4 L_{active} N_{conductors}}{128 \rho} \quad (4)$$

Figure 8 shows the total copper losses (Eddy Current (4) + Resistive Losses (3)) when a stator is constructed from 12 gauge equivalent Litz Wire. The figure demonstrates that for two typical loading conditions the selection of a Litz wire strand size between 33 and 38 gauges would be sensible.

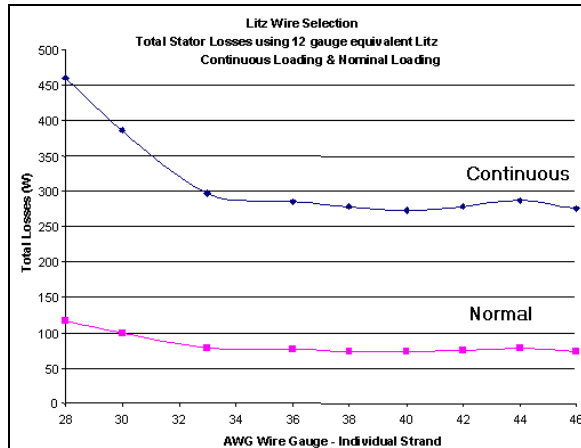


Fig. 8. Total stator copper losses Vs wire gauge.

5. MACHINE SPECIFICATIONS

Number of Phases	3
Number of Poles	24
Peak Air Gap Flux Density	0.56 T
Air-Gap Length	8 mm
Stator Thickness	6 mm
Litz Wire	38 gauge
Winding Fill Factor	38%
Magnet Dimensions (mm)	50 x 20 x 12
Magnet Mass	2.13 kg
Active mass	7 kg
Complete Motor Weight	10 kg

Table 2. Motor Specifications.

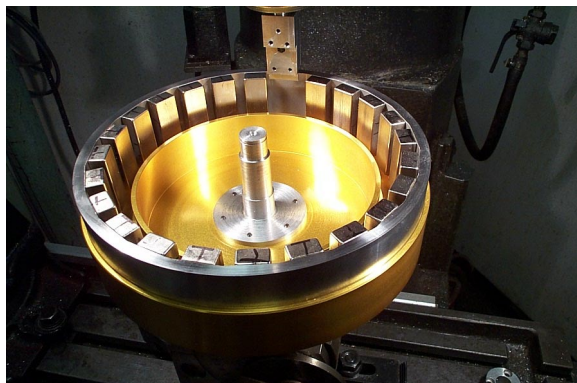


Fig. 9. The final magnet being bonded in position.

4. CONCLUSION

The analysis demonstrates that a relatively large air-gap produces both a higher specific torque and efficiency. The analysis considers resistive losses

and eddy current losses, other losses such as windage and bearing losses will be found experimentally and presented in future publications.

The radial flux topology presented allows for high-speed operation and was shown to deliver a machine with a high power density and a relatively low magnetic material requirement.

6. REFERENCES

- [1] Lovins, A.B., "Hypercars: The Next Industrial Revolution", 13th International Electric Vehicle Symposium (EVS-13), Osaka, Japan. 1996
- [2] Simpson, A.G., Greaves, M.C., and Walker G.R., "Migrating to a sustainable energy system: Distributed Generation and storage, fuel cells and hypercars", AUPEC, Brisbane, Australia 2000. p. 289-94
- [3] Caricchi, F., Crescimbeni, F., Hororati, O., Baianco, G.L., and Santini, E., "Performance of Coreless-Winding Axial-Flux Permanent-Magnet Generator With Power Output at 400 Hz, 3000 r/min", IEEE Transactions on Industrial Applications, Vol. 34, No. 6, November/December 1998.
- [4] Lovatt, H.C., Ramsden, V.S., and Mecrow, B.C., "Design of an in-wheel motor for a solar-powered electric vehicle", IEE Proc.-Electr. Power Appl, Vol. 145, No. 5, September 1998.
- [5] Jensen, C.C., Profumo, F., and Lipo, T.A., "A Low-Loss Permanent-Magnet Brushless dc Motor Utilizing Tape Wound Amorphous Iron", IEEE Transactions on Industrial Applications, Vol. 28, No. 3, May/June 1992.
- [6] Caricchi, F., Mezzetti, F., and Santini, E., "Multistage Axial-Flux PM Machine for Wheel Direct Drive", IEEE Transactions on Industrial Applications, Vol. 32, No. 4, July/August 1996.
- [7] Lambard, N.F., and Kamper, M.J., "Analysis and performance of an Ironless Stator Axial Flux PM Machine", IEEE Transactions on Energy Conversion, Vol. 14, No. 4, December 1999.
- [8] Carter, G.W., "The Electromagnetic Field in its Engineering" Aspects. (Longmans, 2nd ed., 1967), p. 254.